

# Performance of Satellite UWOC Network with Generalized Boresight Error and AWGGN

Tao TENG, Ansu HE

Nanjing University of Aeronautics and Astronautics, Yudao St. 29, Nanjing, Jiangsu Province, China

taoteng@nuaa.edu.cn, heansu8125@nuaa.edu.cn

Submitted May 5, 2023 / Accepted October 30, 2023 / Online first November 13, 2023

**Abstract.** *This paper investigates a dual-hop satellite-marine communication network that employs mixed radio-frequency/underwater wireless optical communication (RF/UWOC). The study focuses on investigating the impacts of non-zero pointing errors and the additive white generalized Gaussian noise (AWGGN) on the dual-hop system. To address the challenge of computing the probability density function (PDF) for the UWOC system with non-zero boresight error, we apply the Laplace transformation and the generalized integro exponential function. Next, we utilize the generalized Gaussian noise to calculate the signal-to-noise ratio (SNR) and the conditional bit error rate (BER). Then, we present system performance metrics such as the outage probability (OP) and BER. We also calculate the asymptotic analysis of the OP and BER by considering poles coinciding, resulting in the proposal of four asymptotic formulas to gain additional insights into the diversity gain. Finally, we provide simulation results that analyze the performance of the proposed satellite-marine network with different system parameters, such as boresight displacements and bubble levels, and validate the accuracy of the numerical results.*

## Keywords

Dual-hop RF/UWOC transmission, decode-and-forward relay, performance analysis, satellite-marine communication network

## 1. Introduction

In recent years, underwater wireless optical communication (UWOC) has gained significant attention in oceanography for applications such as data collection, disaster detection, and military surveillance [1], [2]. Satellite-assisted marine communication is crucial in providing stable and seamless connections, offering wide coverage and flexible network deployment.

However, the combination of the satellite and marine UWOC has not been fully studied. Several papers investigated the data exchange between terrestrial and underwater

wireless networks by using a mixed radio-frequency/optical communication (RF/UWOC) system. The terrestrial network transmits the signal to a buoy relay or a moving ship using an RF link. The relay then converts the electrical signal and retransmits it to the underwater equipment using optical communication. In [3], the authors investigated a dual-hop RF/UWOC system with a fixed gain amplify-and-forward (AF) relay, in which the RF link experienced generalized  $K$  fading. They derived the outage probability (OP), bit error rate (BER), and ergodic capacity (EC) for the system. Furthermore, in [4], the authors analyzed the secrecy performance of an RF/UWOC network using decode-and-forward (DF) relaying. In this case, the RF link undergoes  $\alpha - \mu$  fading, and they deduced the secrecy outage probability of the proposed system. They also analyzed the asymptotic expression at a high signal-to-noise ratio (SNR) to find a suboptimal transmitting power. To explore additional perspectives, [5] considered using an unmanned aerial vehicle (UAV) as the transmitter and analyzed the optimal altitude by considering the elevation angle.

The combination of the satellite and marine UWOC needs to consider the impact of non-zero boresight error and generalized Gaussian noise. Most of the previous studies have focused on zero boresight error. However, due to the motion and sway of the relay, non-zero boresight error remains significant in marine optical communication. The impulsive noise over satellite communication and complex underwater communication environment requires the noise to be modeled as additive white generalized Gaussian noise (AWGGN), most papers considering the additive white Gaussian noise (AWGN) may not be appropriate. The above two key problems motivate the investigation.

The closed-form probability density function (PDF) and cumulative density function (CDF) of the non-zero boresight error over the underwater optical channel have not been proposed. In [6], the authors approximated the non-zero boresight PDF with a modified Rayleigh distribution. In [7], the authors derived the closed-form OP and EC with non-zero boresight error using Laplace manipulation. Yue Wang et al. in [8] obtained the closed-form PDF and CDF of non-zero boresight free space optical (FSO) through mathematical analysis. Meanwhile, the system performance of the dual-hop

satellite marine communication with AWGGN is not investigated. Authors in the [9] investigated the performance of reconfigurable intelligence surface (RIS) - assisted communication with the assumption of AWGGN, [10] derived the BER in the presence of AWGGN in the underwater acoustic channel, and [11] researched the average BER with a generalized fading channel and AWGGN. Thus, in this paper, we consider the impact of non-zero boresight pointing error and generalized Gaussian noise on the satellite-UWOC communication. The contributions of this paper are as follows:

1) A hybrid satellite UWOC system is investigated, in which the satellite transmits signals to an autonomous underwater vehicle (AUV) with an over-sea relay. To account for the impact of non-zero boresight error on underwater wireless optical transmission, we derive the closed-form PDF and CDF of the SNR by utilizing Laplace substitution and generalized integro-exponential functions.

2) With the calculated PDF and CDF, we derive the analytical expressions of the OP and BER of the proposed dual-hop network by considering the non-zero boresight and AWGGN. The asymptotic OP and asymptotic BER formulas by asymptotically expanding the Fox-H function at high SNR regions are deduced. We analyze the diversity gain of the proposed system.

3) We simulate the system performance under different bubble levels (BL), boresight displacements, and AWGGN parameters. The numerical results are validated with the simulations.

## 2. Network Model

### 2.1 System Model

We consider a downlink communication network that combines satellite and UWOC. The system comprises a satellite, denoted by  $s$ , an AUV, denoted by  $d$ , and an over-sea ship station, denoted by  $r$ , which acts as a relay. In the first hop, the DF relay strategy is used at  $r$  to receive the satellite signal. The RF signal is then converted into an underwater optical signal, which is forwarded to the AUV in the second hop. The satellite  $s$  has a single antenna, whereas  $r$  has a single RF receive antenna and a single transmit aperture. Likewise, the AUV is equipped with a single receive aperture.

In the first RF transmission slot, the received signal at  $r$  can be written as

$$y_{sr} = \sqrt{p_s G_{sr}} h_{sr} x_s + n_r \quad (1)$$

where  $p_s$  denotes the sending power of  $s$ ,  $G_{sr}$ ,  $h_{sr}$  represent the propagation gain and fading channel, respectively. The symbol  $x_s$  has a unit energy, and  $n_r$  denotes the generalized Gaussian noise.

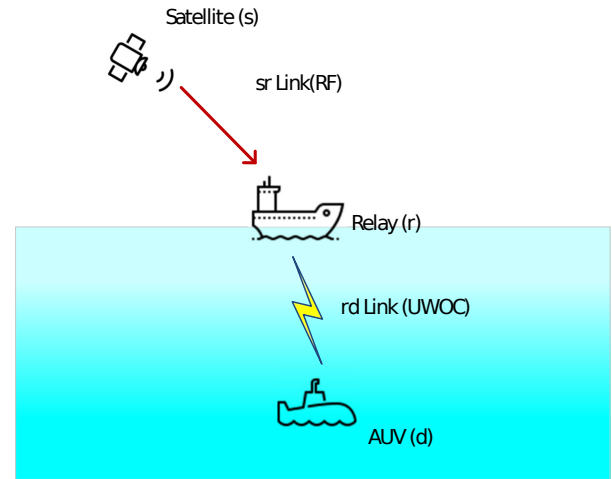


Fig. 1. Dual-hop satellite UWOC system model.

Considering the complex marine communication environment and impulsive noise, we can express the PDF of the AWGGN  $n$  as:

$$f(n|\alpha, \sigma) = \frac{\alpha \Lambda}{2\Gamma(1/\alpha)} \exp(-\Lambda^\alpha |n|^\alpha) \quad (2)$$

where  $\Lambda = \Lambda_0/\sigma$ ,  $\Lambda_0 = \sqrt{\Gamma(3/\alpha)/\Gamma(1/\alpha)}$  [9]. Here,  $\alpha$  and  $\sigma$  represent the shaping parameter and the noise variance, respectively. If we set  $\alpha = 2$  and  $\sigma = \sqrt{2}$ ,  $n$  can be simplified as AWGN. Therefore, by defining the noise parameters  $\alpha_r$  and  $\sigma_r$  at  $r$ , the SNR of the first hop can be written as  $\gamma_{sr} = \bar{\gamma}_s G_{sr} |h_{sr}|^2$ , where  $\bar{\gamma}_s = p_s/\sigma_r^2$ .

In the second phase of transmission, the relay receives the RF signal and forwards it to the destination,  $d$ . The received signal at the AUV can be expressed as

$$y_d = \sqrt{p_r} \eta I x_r + n_d \quad (3)$$

where  $p_r$  is the transmitted power,  $\eta$  represents the optical-to-electrical conversion coefficient.  $I$  denotes the channel fading,  $n_d$  represents the AWGGN with parameters  $\alpha_d$  and  $\sigma_d$ .

Two types of optical signal detection techniques, heterodyne detection (HD) and intensity modulation/direct detection (IM/DD) [12], are used in the system. The instantaneous SNR of the second link is calculated as  $\gamma_{rd} = \frac{p_r (\eta I)^r}{\sigma_d^2}$ , where  $r$  indicates the type of detection strategy, i.e., HD ( $r = 1$ ) or IM/DD ( $r = 2$ ). The average electrical SNR is also calculated as  $\mu_{rd} = \frac{\eta^r E[I]^r p_r}{\sigma_d^2}$ . Here,  $E[\cdot]$  denotes the expected value.

### 2.2 Channel Model

The channel fading,  $I$ , can be expressed as the product of  $h_l$ ,  $h_p$ , and  $h_a$ . Here,  $h_l$  denotes the normalized propagation loss, which is deterministic and modeled by the Beer-Lambert law [13].  $h_p$  indicates the non-zero boresight pointing error loss, and  $h_a$  is modeled as a mixture of the exponential-generalized gamma (EGG) distribution, which can be expressed as:

BL	Salinity	$w$	$\lambda$	$a$	$b$	$c$
2.4	Fresh	0.2130	0.3291	1.4299	1.1817	17.1984
2.4	Salty	0.1770	0.4687	0.7736	1.1372	49.1773
16.5	Salty	0.4951	0.1368	0.0161	3.2033	82.1030

**Tab. 1.** Parameters of the EGG distribution for different bubble level (BL) [l/min] versus fresh water and salinity of water [12].

1) Oceanic Turbulence: The mixture EGG distribution has been proposed by the authors in [12] to describe the irradiance fluctuations of the underwater optical signal, which is well-measured by experimental results compared with the exponential-gamma (EG) distribution and the exponential-lognormal distribution. The PDF of the mixture EGG distribution can be formulated as:

$$f_{h_a}(h_a) = \frac{w}{\lambda} \exp\left(-\frac{h_a}{\lambda}\right) + \frac{(1-w)c}{b^{ac}\Gamma(a)} h_a^{ac-1} \exp\left[-\left(\frac{h_a}{b}\right)^c\right] \quad (4)$$

where the parameters  $w$ ,  $\lambda$ ,  $a$ ,  $b$ , and  $c$  are associated with the attenuation coefficients of EGG fading. The parameters and their corresponding values are listed in Tab. 1.

2) Pointing Error Model: The pointing error model is described in [6]. The radial displacement vector is expressed as  $\mathbf{r} = [r_x, r_y]^T$ , where  $r_x \sim \mathcal{N}(\mu_x, \sigma_x^2)$  and  $r_y \sim \mathcal{N}(\mu_y, \sigma_y^2)$  for the horizontal and elevation axes. The jitter is caused by oceanic turbulence and ship motion over the sea. Assuming  $\sigma_x^2 = \sigma_y^2 = \sigma_s^2$  in the horizontal and elevation axes at  $r$ , the PDF of non-zero boresight pointing error can be expressed as follows:

$$f_{h_p}(h_p) = \frac{\zeta^2 e^{-\frac{s^2}{2\sigma_s^2}}}{A_0^{\zeta^2}} h_p^{\zeta^2-1} I_0\left(\frac{s}{\sigma_s^2} \sqrt{\frac{-w_{z\text{eq}} \ln \frac{h_p}{A_0}}{2}}\right) \quad (5)$$

$$0 \leq h_p \leq A_0$$

where  $s$  denotes the boresight displacement,  $\zeta$  means the degree of the point error,  $\sigma_s^2$  is the variance of jitter,  $A_0$  represents the gathered optical power, and  $w_{z\text{eq}}$  is the beamwidth.

### 3. End to End SNR Statistics

Deriving the closed-form PDF of  $I$  combined with non-zero boresight pointing error  $h_p$  and EGG turbulence fading  $h_a$  is a complex task. In [14], the authors approximated (5) to a modified Rayleigh distribution, which is inaccurate for the statistical characteristics of SNR. Therefore, this section derives the closed-form PDF of  $I$  with the given  $h_l$ ,  $h_a$ ,  $h_p$  as shown in (8) [on the next page]<sup>1</sup>.

Proof: See Appendix A.

<sup>1</sup> The result derived in (8) can be reduced to the PDF of channel fading  $I$  with mixed EGG fading and zero pointing errors in [15, Eq. (8)] by setting  $s = 0$  and  $m = 0$ .

<sup>2</sup> The experimental setup can be viewed at [12]. We will consider the real experiments of the proposed PDF and CDF combination of the non-zero boresight error and AWGGN in the future.

The  $n$ -th moment of  $I$ , denoted by  $E[I^n]$ , can be calculated as 
$$\sum_{m=0}^{\infty} \frac{\zeta^2 e^{-\frac{s^2}{2\sigma_s^2}}}{m! (\zeta^2 + n)^{m+1}} \left(\frac{sw_{z\text{eq}}}{\sqrt{8}\sigma_s^2}\right)^{2m} [w(\lambda A_0 h_l)^n n! + (1-w)(b A_0 h_l)^n \frac{\Gamma(a + \frac{n}{c})}{\Gamma(a)}].$$

Both heterodyne detection and IM/DD can have their average electrical SNR and instantaneous SNR reformulated as  $\frac{\mu_{rd}}{E[I]^r} = \frac{Pr\eta^r}{\sigma_d^2}$  and  $\frac{\gamma_{rd}}{I^r} = \frac{Pr\eta^r}{\sigma_d^2}$ , respectively. Therefore, the relationship between  $I$  and  $\gamma_{rd}$  with respect to  $\mu_{rd}$  can be transformed as  $I = \frac{\gamma_{rd} E[I]}{\mu_{rd}}$  for heterodyne detection and  $I = \sqrt{\frac{\gamma_{rd}}{\mu_{rd}}} E[I]$  for IM/DD. The unified PDF of  $\gamma_{rd}$  is derived in (9) [on the next page], where  $\rho_r = \mu_{r,d}/E[I]^r$ . The CDF of  $\gamma_{rd}$  is then deduced with the aid of [16, Eq.(2.53)] and listed in (10) [on the next page]<sup>2</sup>.

The PDF and CDF of the satellite shadowed-Rician fading can be seen as [17]:

$$f_{\gamma_{sr}}(\gamma) = \sum_{k=0}^{m_s-1} \binom{m_s-1}{k} \frac{\alpha_s \delta_s^k}{\Gamma(1+k) (\bar{\gamma}_s G_{sr})^{k+1}} \times \gamma^k e^{-\frac{\beta_s - \delta_s}{\bar{\gamma}_s G_{sr}} \gamma} \quad (6)$$

$$F_{\gamma_{sr}}(\gamma) = 1 - \sum_{k=0}^{m_s-1} \binom{m_s-1}{k} \frac{\alpha_s \delta_s^k}{(\beta_s - \delta_s)^{k+1}} \times e^{-\frac{(\beta_s - \delta_s)\gamma}{\bar{\gamma}_s G_{sr}}} \sum_{l=0}^k \frac{(\beta_s - \delta_s)^l \gamma^l}{l! (\bar{\gamma}_s G_{sr})^l} \quad (7)$$

where  $\alpha_s = \frac{1}{2b_s} \left(\frac{2b_s m_s}{2b_s m_s + \Omega_s}\right)^{m_s}$ ,  $\beta_s = \frac{1}{2b_s}$ , and  $\delta_s = \frac{\Omega_s}{2b_s(2b_s m_s + \Omega_s)}$ .  $m_s$ ,  $b_s$ ,  $\Omega_s$  are the channel parameters.

## 4. Performance Analysis

In this section, we investigate the impact of non-zero boresight error and non-Gaussian noise on the outage probability and BER of the dual-hop satellite-marine network.

### 4.1 Outage Performance

The outage performance with DF relaying is defined as the minimum of  $\gamma_{sr}$  and  $\gamma_{rd}$  falling below the outage threshold  $r_{\text{th}}$ . Mathematically, it can be expressed as  $P_{\text{out}} = F_{\gamma_{sr}}(r_{\text{th}}) + F_{\gamma_{rd}}(r_{\text{th}}) - F_{\gamma_{sr}}(r_{\text{th}}) F_{\gamma_{rd}}(r_{\text{th}})$ . Substituting (10) and (7) into the formula for  $P_{\text{out}}$ , the closed-form outage probability can be calculated, as shown in (11) [on the next page], where  $\phi(k, l) = \binom{m_s-1}{k} \frac{\alpha_s \delta_s^k}{(\beta_s - \delta_s)^{k+1} l!}$ , and

$$\varphi(m) = \frac{\zeta^2 e^{-\frac{s^2}{2\sigma_s^2}}}{m!} \left(\frac{sw_{z\text{eq}}}{\sqrt{8}\sigma_s^2}\right)^{2m}.$$

$$f_I(I) = \sum_{m=0}^{\infty} \frac{\zeta^2 e^{-\frac{s^2}{2\sigma_s^2}}}{m!} \left( \frac{sw_{zeq}}{\sqrt{8}\sigma_s^2} \right)^{2m} \left[ \frac{w}{I} G_{m+1,m+2}^{m+2,0} \left( \frac{I}{\lambda A_0 h_l} \middle| \begin{matrix} (\zeta^2 + 1) \mathbf{1}_{m+1} \\ 1, \zeta^2 \mathbf{1}_{m+1} \end{matrix} \right) \right. \\ \left. + \frac{(1-w)}{\Gamma(a) c^m I} G_{m+1,m+2}^{m+2,0} \left( \left( \frac{I}{b A_0 h_l} \right)^c \middle| \begin{matrix} \left( \frac{\zeta^2}{c} + 1 \right) \mathbf{1}_{m+1} \\ a, \left( \frac{\zeta^2}{c} \right) \mathbf{1}_{m+1} \end{matrix} \right) \right], \quad (8)$$

$$f_{\gamma_{rd}}(\gamma) = \sum_{m=0}^{\infty} \frac{\zeta^2 e^{-\frac{s^2}{2\sigma_s^2}}}{m!} \left( \frac{sw_{zeq}}{\sqrt{8}\sigma_s^2} \right)^{2m} \left[ \frac{w}{\gamma} H_{m+1,m+2}^{m+2,0} \left( \frac{\gamma}{\lambda^r A_0^r h_l^r \rho_r} \middle| \begin{matrix} (\zeta^2 + 1, r) \mathbf{1}_{m+1} \\ (1, r), (\zeta^2, r) \mathbf{1}_{m+1} \end{matrix} \right) \right. \\ \left. + \frac{(1-w)}{\Gamma(a) c^{m+1} \gamma} H_{m+1,m+2}^{m+2,0} \left( \frac{\gamma}{b^r A_0^r h_l^r \rho_r} \middle| \begin{matrix} \left( \frac{\zeta^2}{c} + 1, \frac{r}{c} \right) \mathbf{1}_{m+1} \\ \left( a, \frac{r}{c} \right), \left( \frac{\zeta^2}{c}, \frac{r}{c} \right) \mathbf{1}_{m+1} \end{matrix} \right) \right], \quad (9)$$

$$F_{\gamma_{rd}}(\gamma) = \sum_{m=0}^{\infty} \frac{\zeta^2 e^{-\frac{s^2}{2\sigma_s^2}}}{m!} \left( \frac{sw_{zeq}}{\sqrt{8}\sigma_s^2} \right)^{2m} \left[ wr H_{m+2,m+3}^{m+2,1} \left( \frac{\gamma}{\lambda^r A_0^r h_l^r \rho_r} \middle| \begin{matrix} (1, r), (\zeta^2 + 1, r) \mathbf{1}_{m+1} \\ (1, r), (\zeta^2, r) \mathbf{1}_{m+1}, (0, r) \end{matrix} \right) \right. \\ \left. + \frac{(1-w)r}{\Gamma(a) c^{m+2}} H_{m+2,m+3}^{m+2,1} \left( \frac{\gamma}{b^r A_0^r h_l^r \rho_r} \middle| \begin{matrix} \left( 1, \frac{r}{c} \right), \left( \frac{\zeta^2}{c} + 1, \frac{r}{c} \right) \mathbf{1}_{m+1} \\ \left( a, \frac{r}{c} \right), \left( \frac{\zeta^2}{c}, \frac{r}{c} \right) \mathbf{1}_{m+1}, \left( 0, \frac{r}{c} \right) \end{matrix} \right) \right], \quad (10)$$

$$P_{\text{out}} = 1 + \sum_{k=0}^{m_s-1} \sum_{l=0}^k \sum_{m=0}^{\infty} \frac{\phi(k, l) \varphi(m)}{\bar{\gamma}_s^l G_{sr}^l} r_{\text{th}}^l e^{-\frac{(\beta_s - \delta_s) r_{\text{th}}}{\bar{\gamma}_s G_{sr}}} \left[ wr H_{m+2,m+3}^{m+2,1} \left( \frac{r_{\text{th}}}{\lambda^r A_0^r h_l^r \rho_r} \middle| \begin{matrix} (1, r), (\zeta^2 + 1, r) \mathbf{1}_{m+1} \\ (1, r), (\zeta^2, r) \mathbf{1}_{m+1}, (0, r) \end{matrix} \right) \right. \\ \left. + \frac{(1-w)r}{\Gamma(a) c^{m+2}} H_{m+2,m+3}^{m+2,1} \left( \frac{r_{\text{th}}}{b^r A_0^r h_l^r \rho_r} \middle| \begin{matrix} \left( 1, \frac{r}{c} \right), \left( \frac{\zeta^2}{c} + 1, \frac{r}{c} \right) \mathbf{1}_{m+1} \\ \left( a, \frac{r}{c} \right), \left( \frac{\zeta^2}{c}, \frac{r}{c} \right) \mathbf{1}_{m+1}, \left( 0, \frac{r}{c} \right) \end{matrix} \right) \right] - \sum_{k=0}^{m_s-1} \sum_{l=0}^k \frac{\phi(k, l)}{\bar{\gamma}_s^l G_{sr}^l} r_{\text{th}}^l e^{-\frac{(\beta_s - \delta_s) r_{\text{th}}}{\bar{\gamma}_s G_{sr}}}. \quad (11)$$

## 4.2 Asymptotic Outage Probability

The current formulation of (11) is convoluted and does not provide any meaningful insights. Therefore, the asymptotic OP can be utilized as an alternative approach to assess the system performance at high SNR regions with a lower computational burden.

For DF relaying, the asymptotic OP can be simplified as  $P_{\text{out}}^{\text{asy}} = F_{\gamma_{sr}}^{\text{asy}}(r_{\text{th}}) + F_{\gamma_{rd}}^{\text{asy}}(r_{\text{th}})$ . When  $\bar{\gamma}_s$  turns to infinity,  $F_{\gamma_{sr}}^{\text{asy}}(r_{\text{th}}) \approx \frac{\alpha_s}{\bar{\gamma}_s G_{sr}} r_{\text{th}}$ . The asymptotic OP of  $F_{\gamma_{rd}}^{\text{asy}}(r_{\text{th}})$  is derived at Tab. 2.

Proof: See Appendix B.

*Remark:* The diversity gain of the asymptotic OP,  $P_{\text{out}}^{\text{asy}}$ , can be derived as  $\min \left\{ 1, \frac{1}{r}, \frac{\zeta^2}{r} \right\}$ , taking into account the restrictions of the four cases on  $F_{\gamma_{rd}}(r_{\text{th}})$  and the asymptotic OP of  $F_{\gamma_{sr}}^{\text{asy}}(r_{\text{th}})$ . It is worth noting that the diversity gain of the dual-hop satellite UWOC system is dependent on the optical modulation method and the degree of the point error, whereas the boresight displacement has no impact on the diversity gain.

## 4.3 Bit Error Rate

In this subsection, we aim to evaluate the average BER performance of the satellite marine network under a generalized Gaussian noise model. The BER can be expressed as [15]:

$$P_e \approx P_{e, sr} + P_{e, rd} \quad (12)$$

where  $P_{e, sr}$  and  $P_{e, rd}$  are the BER of the first transmission hop and the second link, respectively.

Furthermore, the conditional BER can be expressed as  $\Pr(e|\gamma) = \delta \sum_{n=1}^Q Q_{\alpha}(\sqrt{q_n \gamma})$  [12]. The generalized gaussian Q-function is given by  $Q_{\alpha}(x) = \frac{1}{2\Gamma(\frac{1}{\alpha})} H_{1,2}^{2,0} \left( \Lambda_0^{\alpha} x^{\alpha} \middle| \begin{matrix} (1, 1) \\ (0, 1), \left( \frac{1}{\alpha}, 1 \right) \end{matrix} \right)$ , where parameters  $\alpha, \Lambda_0$  have been illustrated in (2). The parameters  $\delta, Q, q_n$  are related to the modulation technique, as shown in Tab. 3.

Therefore, by utilizing [18, Eq. (2.25.1)] along with (9) and substituting (6) into the conditional BER formula, we can derive a closed-form expression for  $P_e$ , which is given by (13) [on the next page].

Asymptotic outage probability expressions of $F_{\gamma_{rd}}(r_{th})$		Conditions
$\sum_{m=0}^{\infty} \frac{\zeta^2 e^{-\frac{\zeta^2}{2\sigma_s^2}}}{m!} \left(\frac{sw_{zeq}}{\sqrt{8}\sigma_s^2}\right)^{2m} \left[ wr \tau_{10}(m) \left(\frac{r_{th}}{\lambda^r A_0^r h_l^r \rho_r}\right)^{\frac{1}{r}} + \frac{(1-w)r \tau_{20}(m)}{\Gamma(a) c^{m+2}} \left(\frac{r_{th}}{b^r A_0^r h_l^r \rho_r}\right)^{\frac{\zeta^2}{r}} \log^m \left(\frac{r_{th}}{b^r A_0^r h_l^r \rho_r}\right) \right]$		$1 < \zeta^2, a \geq \frac{\zeta^2}{c}$
$\sum_{m=0}^{\infty} \frac{\zeta^2 e^{-\frac{\zeta^2}{2\sigma_s^2}}}{m!} \left(\frac{sw_{zeq}}{\sqrt{8}\sigma_s^2}\right)^{2m} \left[ wr \tau_{10}(m) \left(\frac{r_{th}}{\lambda^r A_0^r h_l^r \rho_r}\right)^{\frac{1}{r}} + \frac{(1-w)r \tau_{21}(m)}{\Gamma(a) c^{m+2}} \left(\frac{r_{th}}{b^r A_0^r h_l^r \rho_r}\right)^{\frac{\zeta^2}{r}} \right]$		$1 < \zeta^2, a < \frac{\zeta^2}{c}$
$\sum_{m=0}^{\infty} \frac{\zeta^2 e^{-\frac{\zeta^2}{2\sigma_s^2}}}{m!} \left(\frac{sw_{zeq}}{\sqrt{8}\sigma_s^2}\right)^{2m} \left[ wr \tau_{11}(m) \left(\frac{r_{th}}{\lambda^r A_0^r h_l^r \rho_r}\right)^{\frac{1}{r}} \log^m \left(\frac{r_{th}}{\lambda^r A_0^r h_l^r \rho_r}\right) + \frac{(1-w)r \tau_{21}(m)}{\Gamma(a) c^{m+2}} \left(\frac{r_{th}}{b^r A_0^r h_l^r \rho_r}\right)^{\frac{\zeta^2}{r}} \right]$		$1 \geq \zeta^2, a < \frac{\zeta^2}{c}$
$\sum_{m=0}^{\infty} \frac{\zeta^2 e^{-\frac{\zeta^2}{2\sigma_s^2}}}{m!} \left(\frac{sw_{zeq}}{\sqrt{8}\sigma_s^2}\right)^{2m} \left[ wr \tau_{11}(m) \left(\frac{r_{th}}{\lambda^r A_0^r h_l^r \rho_r}\right)^{\frac{1}{r}} \log^m \left(\frac{r_{th}}{\lambda^r A_0^r h_l^r \rho_r}\right) + \frac{(1-w)r \tau_{20}(m)}{\Gamma(a) c^{m+2}} \left(\frac{r_{th}}{b^r A_0^r h_l^r \rho_r}\right)^{\frac{\zeta^2}{r}} \log^m \left(\frac{r_{th}}{b^r A_0^r h_l^r \rho_r}\right) \right]$		$1 \geq \zeta^2, a \geq \frac{\zeta^2}{c}$

Tab. 2. Asymptotic OP for different conditions.

Modulation	$\delta$	$q_k$	$Q$	Detection type
OOK	1	1/2	1	IM/DD
BPSK	1	2	1	Heterodyne
MPSK	$\frac{2}{\max(\log_2 M, 2)}$	$2\sin^2\left(\frac{(2k-1)\pi}{M}\right)$	$\max\left(\frac{M}{4}, 1\right)$	Heterodyne
MQAM	$\frac{4}{\log_2 M \left(1 - \frac{1}{\sqrt{M}}\right)}$	$\frac{3(2k-1)^2}{M-1}$	$\frac{\sqrt{M}}{2}$	Heterodyne

Tab. 3. Parameters for different modulations with IM/DD or Heterodyne detection.

$$P_e = \sum_{n=1}^Q \sum_{m=0}^{\infty} \frac{\varphi(m) \delta}{\alpha_d \Gamma\left(\frac{1}{\alpha_d}\right)} \left[ w H_{m+3, m+3}^{m+2, 2} \left( \frac{1}{\lambda^r A_0^r h_l^r \rho_r q_n \Lambda_0^2} \middle| \begin{matrix} \left(1, \frac{2}{\alpha_d}\right), \left(1 - \frac{1}{\alpha_d}, \frac{2}{\alpha_d}\right), (1 + \zeta^2, r) \mathbf{1}_{m+1} \\ (1, r), (\zeta^2, r) \mathbf{1}_{m+1}, \left(0, \frac{2}{\alpha_d}\right) \end{matrix} \right) + \right. \quad (13)$$

$$\left. \frac{(1-w)}{\Gamma(a) c^{m+1}} H_{m+3, m+3}^{m+2, 2} \left( \frac{1}{b^r A_0^r h_l^r \rho_r q_n \Lambda_0^2} \middle| \begin{matrix} \left(1, \frac{2}{\alpha_d}\right), \left(1 - \frac{1}{\alpha_d}, \frac{2}{\alpha_d}\right), \left(1 + \frac{\zeta^2}{c}, \frac{r}{c}\right) \mathbf{1}_{m+1} \\ \left(a, \frac{r}{c}\right), \left(\frac{\zeta^2}{c}, \frac{r}{c}\right) \mathbf{1}_{m+1}, \left(0, \frac{2}{\alpha_d}\right) \end{matrix} \right) \right]$$

$$+ \sum_{n=1}^Q \sum_{k=0}^{m_s-1} \binom{m_s-1}{k} \frac{\alpha_s \delta_s^m \delta}{2k! \Gamma\left(\frac{1}{\alpha_r}\right) (\beta_s - \delta_s)^{k+1}} H_{2,2}^{1,2} \left( \left( \frac{\beta_s - \delta_s}{\Lambda_0^2 q_n \tilde{\gamma}_s G_{sr}} \right)^{\frac{\alpha_r}{2}} \middle| \begin{matrix} (1, 1), \left(1 - \frac{1}{\alpha_r}, 1\right) \\ (1+k, \frac{\alpha_r}{2}), (0, 1) \end{matrix} \right).$$

#### 4.4 Asymptotic Bit Error Rate

The asymptotic BER can be obtained using the same approach as presented in Tab. 2, which can be expressed as  $P_e^{\text{asy}} \approx P_{e, sr}^{\text{asy}} + P_{e, rd}^{\text{asy}}$ . To simplify the analysis, we consider the case where  $1 < \zeta^2$  and  $a \geq \frac{\zeta^2}{c}$ . In this case, the expression for  $P_e^{\text{asy}}$  can be written as follows:

$$P_{e, rd}^{\text{asy}} \approx \sum_{n=1}^Q \sum_{k=0}^{m_s-1} \frac{\tau_3(k)}{(\Lambda_0^2 q_n \tilde{\gamma}_s G_{sr})^{k+1}} +$$

$$\sum_{n=1}^Q \sum_{m=0}^{\infty} \left[ \frac{\tau_4(m)}{(\lambda^r A_0^r h_l^r \rho_r q_n \Lambda_0^2)^{\frac{1}{r}}} + \frac{\tau_5(m) \log^m \left( \frac{1}{b^r A_0^r h_l^r \rho_r q_n \Lambda_0^2} \right)}{(b^r A_0^r h_l^r \rho_r q_n \Lambda_0^2)^{\frac{\zeta^2}{r}}} \right], \text{ the}$$

parameters are shown as  $\tau_3(k) = \binom{m_s-1}{k} \frac{\alpha_s \delta_s^m \Gamma\left(\frac{3+2k}{\alpha_r}\right)}{(1+k) 2k! \Gamma\left(\frac{1}{\alpha_r}\right)}$ ,

$$\tau_4(m) = \frac{\alpha \Gamma\left(\frac{1}{\alpha} + \frac{2}{\alpha r}\right) w \varphi(m) \delta}{2 \zeta^{2m+2} \alpha_d \Gamma\left(\frac{1}{\alpha_d}\right)}, \text{ and the last term is } \tau_5(m) =$$

$$\frac{(-1)^m \alpha r}{2 \zeta^{2m} m! r^{m+1}} \Gamma\left(a - \frac{\zeta^2}{c}\right) \Gamma\left(\frac{r+2\zeta^2}{\alpha r}\right) \frac{(1-w) \varphi(m) \delta}{\alpha_d \Gamma\left(\frac{1}{\alpha_d}\right) \Gamma(a)}, \text{ the diversity}$$

gain of the BER is  $\min\left\{1, \frac{1}{r}, \frac{\zeta^2}{r}\right\}$ .

#### 5. Numerical Results and Discussions

In this section, Monte Carlo simulations are performed to analyze the OP and BER. The real measure data is generated by MATLAB, which comes from [12]. The satellite-relay link experiences SR fading with parameters (1, 0.063, 0.0007) and (5, 0.251, 0.279) indicating frequent heavy shadowing and infrequent light shadowing, respectively. The other parameters are shown in Tab. 4.

Figure 2 depicts the PDF of the system with non-zero-boresight pointing error, using the HD method and a comparison with the modified Rayleigh distribution from [14]. Equation (9) represents the theoretical formula, which shows good agreement with the simulation results, validating our derivation. Our analysis demonstrates that the approximation result is insufficient for system performance analysis, and we employ a finite terms summation, such as 15 terms, in our theoretical calculation. These results indicate that the computational burden is low for using (9).

As is shown from Figs. 3–5, we investigate the impact of channel parameters of EGG fading on system performance with  $r = 1$  and  $r_{th} = 0.01$ . The theoretical formula and asymptotic OP can be viewed in (10) and Tab. 2, respectively. As shown in Tab. 1, we simulate three sets of parameters:  $w, \lambda, a, b$ , and  $c$ . 'Salty water BL = 2.4' and 'Fresh water BL = 2.4' indicate  $a \geq \frac{\zeta^2}{c}$ , while 'Salty water BL = 16.5' results in  $a < \frac{\zeta^2}{c}$ . Figure 3 confirms the accuracy of the asymptotic OP. Increasing the BL from 2.4 (L/min) to 16.5 (L/min) degrades the performance of the OP. Moreover, we observe that the salinity of the water affects the system's performance. The OP of  $\gamma_{rd}$  increases for freshwater compared to saline water. Meanwhile, the investigation of changing the temperature of the sea and then changing the salinity of the water is depicted in Fig. 4 and Fig. 5 with fixed SNR at 20 dB. It is obvious that the OP of fresh water is better than that of fresh water. The OP increases with the increase of the bubble level. For the fixed bubble level BL = 2.4 m, the OP becomes worse when the temperature gradient increases.

Parameter	Value
Propagation gain $G_{sr}$	-50.5 dBi [19]
AWGGN $\alpha_r, \alpha_d, \sigma_r, \sigma_d$	4, 4, 2.4, 2.4 [11]
Boresight error $r, \sigma_s, w_z$	10 cm, 10, 100 cm [6]

Tab. 4. Simulation parameters.

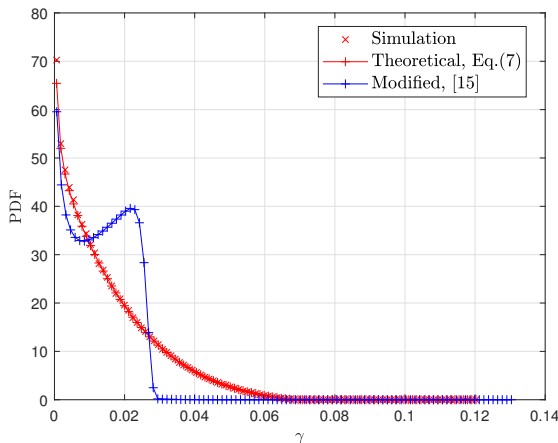


Fig. 2. Simulation of the PDF compared with the modified Rayleigh approximation.

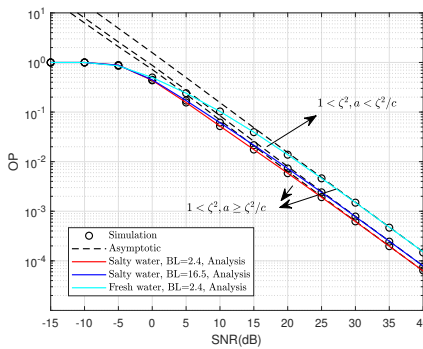


Fig. 3. Comparison of the OP with different salinity of water and bubble levels.

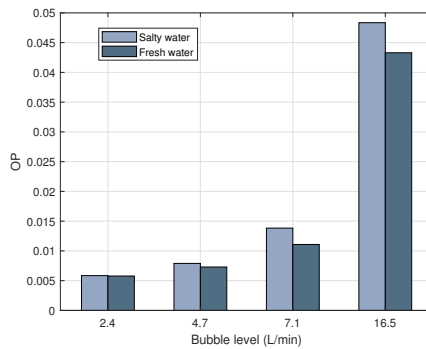


Fig. 4. Comparison of the OP with salinity of water and fixed transmitting power.

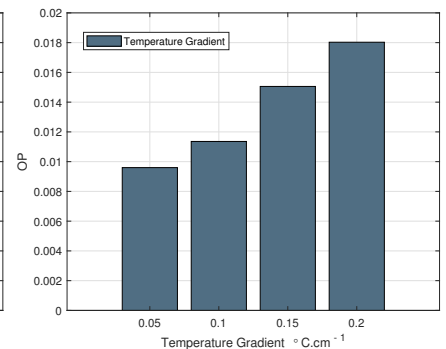


Fig. 5. Comparison of the OP with temperature gradient and fixed transmitting power.

The impact of the detection method and channel conditions on the shadowed-Rician fading is illustrated in Fig. 6. The OP performance of  $r = 2$  is observed to be worse than that of  $r = 1$ , indicating that the HD technology can reduce the OP caused by UWOC. Additionally, the OP of the dual-hop system in weak shadowed-Rician turbulence ( $m_s = 1$ ) is lower than that in the strong shadowed-Rician fading channel ( $m_s = 5$ ). The plot also includes OP expressions at high SNR, and the OP performance with  $r = 2$  and  $s = 0$  is compared to the system considering zero boresight pointing error in UWOC. It is evident that the OP of zero boresight with  $r = 2, m_s = 1$ , and  $s = 0$  is better than that of non-zero boresight with  $r = 2, m_s = 1$ , and  $s = 0.3$ . Moreover, the SNR gap increases with the decrease of OP, and the investigation of non-zero pointing is crucial to evaluate the performance of the proposed dual-hop satellite marine system. The diversity gain of the system can be computed using the nodes (50, 0.0146) and (60, 0.00147) for HD and (50, 0.04137) and (60, 0.01105) for IM/DD, respectively. The diversity gain is calculated as 1 and 1/2, respectively, which matches the theoretical result  $\min \left\{ 1, \frac{1}{r}, \frac{\zeta^2}{r} \right\}$ .

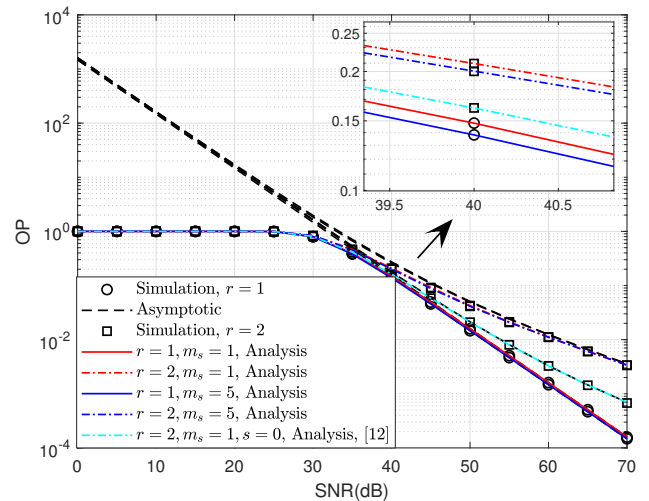


Fig. 6. Comparison of the dual-hop outage probability with different parameters of shadowed-Rician fading and zero/non-zero boresight error.

The performance of the average BER is shown in Fig. 7 for different parameters of the AWGGN, with  $\alpha = 2$  and  $\sigma = \sqrt{2}$  as the reference case for AWGN. It is observed that the BER deteriorates as the value of  $\alpha$  decreases from 4 to 2, and as the value of  $\sigma$  decreases from 2.4 to  $\sqrt{2}$ . These results indicate that a higher value of  $\alpha$  can decrease the error rate, while a higher value of  $\sigma$  may increase the BER. The change from  $\alpha = 4$  to  $\alpha = 2$  causes a gap of almost 1 dB in BER, while the change from  $\sigma = 2.4$  to  $\sigma = \sqrt{2}$  causes a gap of almost 5 dB. The comparison between on-off keying (OOK) modulation with  $r = 2$  and 4-quadrature amplitude modulation (4QAM) is also presented, and the results show that the 4QAM transmission outperforms the OOK transmission. These findings highlight the significant impact of the complex mixed satellite UWOC environment.

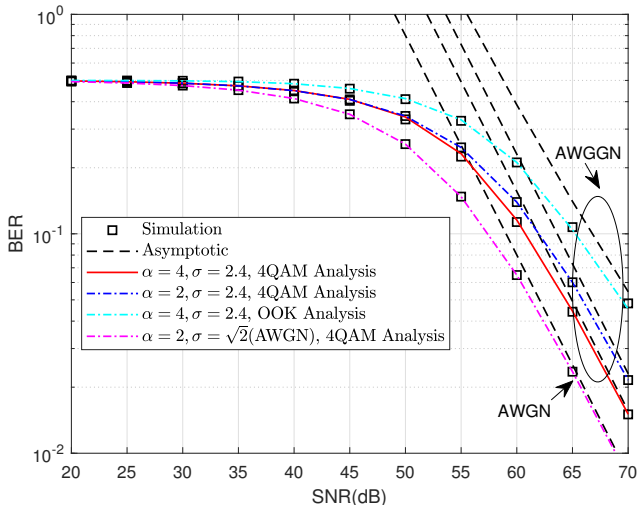


Fig. 7. Comparison of the BER with different parameters in  $\alpha$ ,  $\sigma$ , and modulation modes.

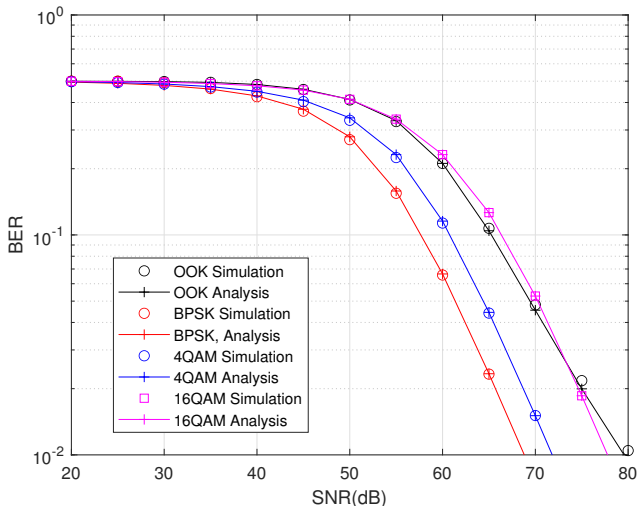


Fig. 8. Comparison of the BER with different modulation schemes.

Finally, the BER performance with different modulation methods is presented in Fig. 8. It can be found that the BER performance of BPSK is superior to the other methods. However, the spectrum efficiency of BPSK is lower. Moreover, the BER performance of OOK is worse, which is the drawback of the simple optical detection method. The BER performance of 4QAM and 16QAM are also simulated, which is evident in the accuracy of the deduced closed-form BER formulas. The balancing between simple detection, the best BER performance, and the spectrum efficiency should be considered in the real satellite-UWOC communication network.

### 6. Conclusion

This paper investigates the performance of a dual-hop satellite-marine RF/UWOC system, taking into account the effects of non-zero pointing errors and non-Gaussian noise in marine communication. We propose a method to derive closed-form PDF and CDF formulas of the SNR, which are then used to calculate analytical expressions of OP and BER. The asymptotic OP and BER are analyzed by considering the poles coinciding. The results of this study indicate that the performance gap increases with the SNR concerning the zero and non-zero boresight errors. Thus, it is crucial to consider non-zero errors when evaluating the performance of marine communication. Additionally, the system's performance is affected by the parameters of the AWGGN. This work will aid in the application of the mixed RF/UWOC network with the performance evaluation and the balancing of the detection techniques, BER performance, and spectrum efficiency.

### Acknowledgments

This work was funded by the Postgraduate Research & Practice Innovation Program of Jiangsu Province (No. KYCX20\_0202).

### References

- [1] SHIHADA, B. Aqua-Fi: Delivering internet underwater using wireless optical networks. *IEEE Communications Magazine*, 2020, vol. 58, no. 5, p. 84–89. DOI: 10.1109/mcom.001.2000009
- [2] WANG, C.-X., HUANG, J., WANG, H., et al. 6G wireless channel measurements and models: Trends and challenges. *IEEE Vehicular Technology Magazine*, 2020, vol. 15, no. 4, p. 22–32. DOI: 10.1109/mvt.2020.3018436
- [3] LI, S., YANG, L., DA COSTA, D. B., et al. Performance analysis of mixed RF-UWOC dual-hop transmission systems. *IEEE Transactions on Vehicular Technology*, 2020, vol. 69, no. 11, p. 14043–14048. DOI: 10.1109/tvt.2020.3029529
- [4] LOU, Y., SUN, R., CHENG, J., et al. Secrecy outage analysis of two-hop decode-and-forward mixed RF/UWOC systems. *IEEE Communications Letters*, 2020, vol. 26, no. 5, p. 989–993. DOI: 10.1109/lcomm.2021.3058988

- [5] YADAV, S., VATS, A., AGGARWAL, M., et al. Performance analysis and altitude optimization of UAV-enabled dual-hop mixed RF-UWOC system. *IEEE Transactions on Vehicular Technology*, 2021, vol. 70, no. 12, p. 12651–12661. DOI: 10.1109/tvt.2021.3118569
- [6] YANG, F., CHENG, J., A. TSIFTSIS, T. Free-space optical communication with nonzero boresight pointing errors. *IEEE Transactions on Communications*, 2014, vol. 62, no. 2, p. 713–725. DOI: 10.1109/tcomm.2014.010914.130249
- [7] UPADHYA, A., GUPTA, J., DWIVEDI, V. K., et al. Impact of RF/IQ imbalance on interference-limited mixed RF/FSO TWR systems with non-zero boresight error. *IEEE Wireless Communications Letters*, 2021, vol. 10, no. 2, p. 416–420. DOI: 10.1109/lwc.2020.3033528
- [8] WANG, Y., WANG, P., LIU, X., et al. On the performance of dual-hop mixed RF/FSO wireless communication system in urban area over aggregated exponentiated Weibull fading channels with pointing errors. *Optics Communications*, 2018, vol. 410, p. 609–616. DOI: 10.1016/j.optcom.2017.10.062
- [9] MOHJAZI, L., BARIAH, L., MUHAIDAT, S., et al. Performance of reconfigurable intelligent surfaces in the presence of generalized Gaussian noise. *IEEE Communications Letters*, 2022, vol. 26, no. 4, p. 773–777. DOI: 10.1109/LCOMM.2022.3145291
- [10] BANERJEE, S., AGRAWAL, M. Underwater acoustic noise with generalized Gaussian statistics: Effects on error performance. In *MTS/IEEE OCEANS - Bergen*. Bergen (Norway), 2013, p. 1–8. DOI: 10.1109/OCEANS-Bergen.2013.6608191
- [11] SOURY, H., YILMAZ, F., ALOUINI, M.-S. Average bit error probability of binary coherent signaling over generalized fading channels subject to additive generalized Gaussian noise. *IEEE Communications Letters*, 2012, vol. 16, no. 6, p. 785–788. DOI: 10.1109/lcomm.2012.040912.112612
- [12] ZEDINI, E., OUBEI, H. M., KAMMOUN, A., et al. Unified statistical channel model for turbulence-induced fading in underwater wireless optical communication systems. *IEEE Transactions on Communications*, 2019, vol. 67, no. 4, p. 2893–2907. DOI: 10.1109/tcomm.2019.2891542
- [13] AMMAR, S., AMIN, O., ALOUINI, M.-S., et al. Energy-aware underwater optical system with combined solar cell and SPAD receiver. *IEEE Communications Letters*, 2022, vol. 26, no. 1, p. 59–63. DOI: 10.1109/lcomm.2021.3127198
- [14] BOLUDA-RUIZ, R., GARCIA-ZAMBRANA, A., CASTILLO-VAZQUEZ, C., et al. Novel approximation of misalignment fading modeled by Beckmann distribution on free-space optical links. *Optics Express*, 2016, vol. 24, no. 3, p. 22635–22649. DOI: 10.1364/oe.24.022635
- [15] LI, S., YANG, L., DA COSTA, D. B., et al. Performance analysis of UAV-based mixed RF-UWOC transmission systems. *IEEE Transactions on Communications*, 2021, vol. 69, no. 8, p. 5559–5572. DOI: 10.1109/tcomm.2021.3076790
- [16] MATHAI, A. M., SAXENA, R. K., HAUBOLD, H. J. *The H-Function: Theory and Applications*. New York (USA): Springer, 2010. ISBN: 9781441909152
- [17] TENG, T. Outage probability and ergodic capacity analysis of satellite-terrestrial NOMA system with mixed RF/mmWave relaying. *Journal of Physics Communications*, 2023, vol. 57, no. C, p. 1–9. DOI: 10.1016/j.phycom.2023.101998
- [18] PRUDNIKOV, A. P., BRYCHKOV, Y. A., MARICHEV, O. I. *Integrals and Series, Vol. 3: More Special Functions*. New York (USA): Gordon and Breach Science Publishers, 1989. ISBN: 9782881246821
- [19] PRUDNIKOV, A. P., BRYCHKOV, Y. A., MARICHEV, O. I., et al. On the performance of cognitive satellite-terrestrial networks. *IEEE Transactions on Cognitive Communications and Networking*, 2017, vol. 3, no. 4, p. 668–683. DOI: 10.1109/tccn.2017.2763619
- [20] GRADSHTEYN, I. S., RYZHIK, I. M. *Table of Integrals, Series, and Products*. Academic Press, 2014. ISBN: 9780123849335
- [21] MILGRAM, M. S. The generalized integro-exponential function. *Mathematics of Computation*, 1985, vol. 44, no. 170, p. 443–458. DOI: 10.1090/s0025-5718-1985-0777276-4
- [22] KILBAS, A. A. *H-Transforms: Theory and Applications*. Boca Raton (FL, USA): CRC Press, 2004. ISBN: 9780429205163

## About the Authors ...

**Tao TENG** received the B.Sc. degree from Jiangsu University, Zhenjiang, China, in 2017. He is currently pursuing the Ph.D. degree with Nanjing University of Aeronautics and Astronautics, Nanjing, China.

**Ansu HE** is currently pursuing her M.Sc. degree with Nanjing University of Aeronautics and Astronautics, Nanjing, China.

## Appendix A: Proof of (8)

To deduce the statistics of  $I = h_a h_p h_l$ , we define the intermediate variable  $z = h_a h_p$ , and the integration transform of  $z$  can be calculated as:

$$f(z) = \int_{\frac{z}{A_0}}^{\infty} \frac{1}{h_a} f_{h_p} \left( \frac{z}{h_a} \right) f_{h_a}(h_a) dh_a \quad (A1)$$

where the low bound of the integration can be obtained with the definition of domain  $h_p \in [0, A_0]$ , then the calculation of  $f(z)$  can be given as (A2) [on the next page].

Equation (A2) holds with the help of the expansion of the  $I_0(x)$  in [20, Eq. (8.402)] as well as utilizing variable transmission  $t = -\ln \frac{I}{A_0 h_a h_l}$ . After performing some mathematical manipulations, the deduction of  $f(z)$  can be transferred to calculate  $\mathcal{I}_1$ .

Next, by resorting to the Laplace transform  $\mathcal{L}\{f(t)\}(s) = F(s)$ , we have  $\mathcal{L}\left(e^{-\frac{z}{\lambda A_0} e^t}\right) = E_{1+s}\left(\frac{z}{\lambda A_0}\right)$  and  $\mathcal{L}\left[e^{-\left(\frac{z}{b A_0}\right)^c} e^{ct}\right] = \frac{1}{c} E_{\frac{c+s}{c}}\left[\left(\frac{z}{b A_0}\right)^c\right]$  as per [20, Eq.(3.331.1)]. The integral term  $\mathcal{I}_1$  can be recalculated shown at step (a) in (A3) [on the next page] with  $\mathcal{L}[t^m f(t)](s) = (-1)^m F^{(m)}(s)$ . Then, by using the definition of generalized integro-exponential function  $E_s^{(m)}(z)$  in [21, Eq.(2.1)], and replacing  $E_s^{(m)}(z)$  to Meijer function in [21, Eq.(2.7.a)], we can obtain  $\frac{\partial^m}{\partial s^m} E_{\frac{c}{c}+1}\left[\left(\frac{z}{b A_0}\right)^c\right] = \frac{(-1)^m \Gamma(m+1)}{c^m} G_{m+1, m+2}^{m+2, 0}\left(z \left| \begin{matrix} s \mathbf{1}_{m+1} \\ 0, (s-1) \mathbf{1}_{m+1} \end{matrix} \right. \right)$ , where  $\mathbf{1}_{m+1}$  denotes the  $(m+1) \times 1$  column vector with element 1, and  $\frac{\partial^m}{\partial s^m} E_{s+1}\left(\frac{z}{\lambda A_0}\right) = \frac{\Gamma(m+1)}{(-1)^m} G_{m+1, m+2}^{m+2, 0}\left(\frac{z}{\lambda A_0} \left| \begin{matrix} s \mathbf{1}_{m+1} \\ 0, (s-1) \mathbf{1}_{m+1} \end{matrix} \right. \right)$ . Thus, the closed-form expression of  $\mathcal{I}_1$  can be obtained as step (b).

$$f(z) = \frac{\zeta^2 e^{-\frac{\zeta^2}{2\sigma_s^2}} z^{\zeta^2-1}}{A_0^{\zeta^2}} \sum_{m=0}^{\infty} \frac{1}{(m!)^2} \left( \frac{sw_{zeq}}{\sqrt{8}\sigma_s^2} \right)^{2m} \left( \frac{z}{A_0} \right)^{-\zeta^2+1} \quad (A2)$$

$$\times \underbrace{\int_0^{\infty} e^{-(\zeta^2-1)t} \left[ \frac{w}{\lambda} e^{-\frac{z}{\lambda A_0} e^t} + \frac{(1-w)c}{b^{ac}\Gamma(a)} \left( \frac{z}{A_0} \right)^{ac-1} e^{(ac-1)t} e^{-\left(\frac{z}{bA_0}\right)^c e^{ct}} \right] t^m dt}_{I_1}.$$

$$I_1 \stackrel{(a)}{=} (-1)^m \frac{\partial^m}{\partial s^m} \left\{ \frac{w}{\lambda} E_{s+1} \left( \frac{z}{\lambda A_0} \right) \Big|_{s=\zeta^2-1} + \frac{(1-w)}{b^{ac}\Gamma(a)} \left( \frac{z}{A_0} \right)^{ac-1} E_{\frac{s}{c}+1} \left[ \left( \frac{z}{bA_0} \right)^c \right] \Big|_{s=\zeta^2-ac} \right\} \quad (A3)$$

$$\stackrel{(b)}{=} \Gamma(m+1) \left[ \frac{w}{\lambda} G_{m+1,m+2} \left( \frac{z}{\lambda A_0} \mid 0, (\zeta^2-1) \mathbf{1}_{m+1} \right) + \frac{(1-w)}{b^{ac}\Gamma(a) c^m} \left( \frac{z}{A_0} \right)^{ac-1} G_{m+1,m+2} \left( \left( \frac{z}{bA_0} \right)^c \mid \left( \frac{\zeta^2}{c} - a + 1 \right) \mathbf{1}_{m+1}, 0, \left( \frac{\zeta^2}{c} - a \right) \mathbf{1}_{m+1} \right) \right].$$

Finally, the expression of (A3) can be simplified with the aid of [20, Eq. (9.31.5)]. Thus, substituting (A3) into (A2) and calculating the integral of  $f_I(I)$  with  $f_I(I) = \frac{1}{h_l} f_z \left( \frac{I}{h_l} \right)$ , the closed-form PDF of  $f_I(I)$  can be expressed as (8).

## Appendix B: Proof of Asymptotic Outage Probability

For  $F_{\gamma_{rd}}^{\text{asy}}(r_{\text{th}})$ , it can be found that some poles of the Fox-H function coincide, such as  $(\zeta^2, r) \mathbf{1}_{m+1}$  and  $\left( \frac{\zeta^2}{c}, \frac{r}{c} \right) \mathbf{1}_{m+1}$  in the Fox-H functions. The asymptotic expression of the  $F_{\gamma_{rd}}(r_{\text{th}})$  can be calculated with Theorem 1.12 in [22]. The follows four cases:  $1 < \zeta^2$  and  $a \geq \frac{\zeta^2}{c}$ ,  $1 < \zeta^2, a < \frac{\zeta^2}{c}$ ,  $1 \geq \zeta^2, a \geq \frac{\zeta^2}{c}$ , and

$1 \geq \zeta^2, a < \frac{\zeta^2}{c}$  are considered. The approximate expressions of  $F_{\gamma_{rd}}(r_{\text{th}})$  can be expressed as Tab. 2, where the parameters  $\tau_{10}(m) = \frac{1}{r(\zeta^2-1)^{m+1}}$ ,  $\tau_{11}(m) = \frac{(-1)^m \Gamma(1-\zeta^2)}{\Gamma(m+1)r^{m+1}\zeta^2}$ ,  $\tau_{20}(m) = \frac{(-1)^m \Gamma\left(a - \frac{\zeta^2}{c}\right) c}{\Gamma(m+1)\zeta^2} \left(\frac{c}{r}\right)^{m+1}$ , and  $\tau_{21}(m) = \frac{c}{ar\left(\frac{\zeta^2}{c} - a\right)^{m+1}}$ . It can

be seen that the approximation expressions shown in Tab. 2 contain log function, which is hard to tackle. Thus the diversity gain can not be calculated directly. In the following, We present an approximation method to deal with this problem with the aid of  $\log x = -\sum_{n=1}^{\infty} \frac{(1-x)^n}{n}$ . When  $x$  tends to 0, the asymptotic OP shown in Tab. 2 can be simplified by comparing  $\left( \frac{r_{\text{th}}}{\lambda^r A_0^r h_l^r \rho_r} \right)^{\frac{1}{r}}$  and  $\left( \frac{r_{\text{th}}}{b^r A_0^r h_l^r \rho_r} \right)^{\frac{\zeta^2}{r}}$ . Thus, the diversity gain of  $F_{\gamma_{rd}}^{\text{asy}}(r_{\text{th}})$  is  $\min \left\{ \frac{1}{r}, \frac{\zeta^2}{r} \right\}$ .